Journal of Materials Chemistry

Cite this: J. Mater. Chem., 2012, 22, 23091

www.rsc.org/materials

PAPER

Graphene oxide oxidizes stannous ions to synthesize tin sulfide–graphene nanocomposites with small crystal size for high performance lithium ion batteries†

Ming Zhang,[ab] Danni Lei,[a] Xinzhi Yu,[a] Libao Chen,[a] Qiuhong Li,[a] Yanguo Wang,[a] Taihong Wang*[a] and Guozhong Cao*[b]

Received 23rd July 2012, Accepted 13th September 2012
DOI: 10.1039/c2jm34864k

This study reports a novel strategy of preparing graphene composites by employing graphene oxide as precursor and oxidizer. It is demonstrated that graphene oxide can oxidize stannous ions to form SnS_2 and is simultaneously reduced to graphene, directly resulting in the formation of SnS_x–graphene ($1 < x < 2$) nanocomposites. The particle size of SnS_x in the nanocomposites is tailored to be about 5 nm, which is much smaller than that obtained in a previous study. As anodic materials for lithium ion batteries, SnS_x–graphene nanocomposites retain a discharge capacity of 860 mA h g^{-1} after 150 cycles at a charge–discharge rate of 0.2 C, higher than the theoretical capacities of SnS_2 (645 mA h g^{-1}) and SnS (782 mA h g^{-1}) based on the traditional mechanism. A possible new mechanism, that Li_2S arising from tin sulfide in the first discharge cycle could be reversibly decomposed at a low potential to storage lithium, is proposed based on experimental results to explain the excellent properties of SnS_x–graphene nanocomposites.

1 Introduction

Graphene, a novel carbon material, possesses excellent properties in many fields. Considerable efforts have been devoted to the synthesis and application of graphene.[1–4] Taking into account its good stability and high conductivity, graphene has been introduced to modify other materials with improved performances in the fields of lithium ion batteries (LIBs),[5,6] ultracapacitors,[7] solar cells,[8] fuel cells,[9] and electronic devices.[10] Graphene composites (GCs), such as metal oxide–graphene, metal–graphene, and polymer–graphene composites, with enhanced performance have been investigated by many authors.[4,11,12] To realize the practical application of GCs, it is of great importance to develop reliable, efficient, environmentally friendly and low-cost strategies for the synthesis of GCs.

Generally, the syntheses of GCs consist of two steps: reducing graphene oxide (GO) and preparing the composites.[4,5] The normal reductants for the reduction of GO, such as sodium borohydride, H_2 and hydrazine, are either hygroscopic or dangerous.[8,10] In addition, most of the two-step approaches are tedious and time-consuming. To improve the synthesis routes to GCs, some one-pot strategies have been developed. For example, GO was reduced to graphene using ascorbic acid along with deposition of ferric ions onto the graphene.[13] Ascorbic acid was employed as an additional reductant in this procedure while its oxidation product was valueless. On the other hand, it should be noted that GO may be used as oxidizers when they are reduced to graphene.[13] As far as we know, there is no research into making use of GO as an oxidizer to form materials.

An important application of GCs is their use as electrode materials for LIBs. A lot of metal oxide–graphene composites with good performance have been investigated,[3,5,12,14] and quite a few studies have been published on the synthesis and application of metal sulfide–graphene in LIBs.[15–18] Among them, tin sulfide–graphene composites are good candidates for the anodes of LIBs with high specific capacity. A case in point is that graphene–SnS_2, synthesized by treating graphene–SnO_2 under a gas mixture of H_2S and Ar, delivered a discharge capacity of 650 mA h g^{-1} after 50 cycles.[15] Hydrothermal methods could also be used to prepare SnS_2–graphene with improved performance.[16–18] It should be noted that the tin sources in those studies were stannic ions, which could not be oxidized by GO. As far as we know, there are few reports about employing GO to oxidize stannous ions to form SnS_x–graphene (SnS_x–G, $1 < x < 2$) nanocomposites, which is an efficient, environmentally friendly and low-cost method.

[a]Key Laboratory for Micro-Nano Optoelectronic Devices of Ministry of Education and State Key Laboratory for Chemo/Biosensing and Chemometrics, Hunan University, Changsha, 410082, China. E-mail: thwang@iphy.ac.cn; Tel: +86-731-88624019
[b]Department of Materials Science and Engineering, University of Washington, Seattle, Washington, 98195, USA. E-mail: gzcao@u.washington.edu; Tel: +1-206-616-9084

† Electronic supplementary information (ESI) available: Details of experiments and TG of SnS_x–G nanocomposites. See DOI: 10.1039/c2jm34864k

In this study, a novel strategy of preparing SnS_2 *via* oxidizing stannous ions by GO is developed for the synthesis of SnS_x–G nanocomposites without an additional reductant for GO. The diameter of SnS_x in nanocomposites is adjusted to be about 5 nm. As anodic materials for LIBs, SnS_x–G nanocomposites maintained a discharge capacity of about 860 mA h g^{-1} after 150 cycles at a charge–discharge rate of 0.2 C. A possible new mechanism of reversibly decomposing Li_2S and alloying with tin for the storage of Li^+ in SnS_x–G nanocomposites is proposed based on experimental results to explain the reason why their performances are so good.

2 Experimental

Materials

Graphite powders were purchased from Alfa Aesar China (Tianjin) Co. Ltd. Stannous chloride dihydrate ($SnCl_2 \cdot 2H_2O$) and thiourea ($CS(NH_2)_2$) were purchased from Sinopharm Chemical Reagent Co. Ltd (Shanghai, China). All other reagents were of analytical grade and used as received without any purification process. The water was Millipore Milli-Q grade with a resistivity larger than 18 MΩ cm^{-1}.

Synthesis of SnS_x–G nanocomposites

GO was fabricated according to previous literature procedures.[14,19] To synthesize SnS_x–G nanocomposites, we prepared a mixture of GO, $SnCl_2 \cdot 2H_2O$ and thiourea with concentrations of 0.5 mg mL^{-1}, 15 mM and 60 mM, respectively. Secondly, the flask was purged with N_2 to eliminate oxygen. Thirdly, the above suspension was transferred into a Teflon-lined stainless steel autoclave and maintained at 453 K for 12 h. After that, the autoclave was cooled to room temperature, and the products were collected and dried. They were noted as SnS_x–G. In a control experiment, the mixture without GO was processed under the same conditions for 12 h. After washing with ethanol and distilled water, the final sample was collected and marked as SnS_x-1.

Materials characterization

The composites were characterized by powder X-ray diffraction using a SIEMENS D5000 X-ray diffractometer with Cu-K_α irradiation (λ = 0.15406 nm), a WQF-410 Fourier transform infrared spectrophotometer, a thermogravimetric analysis (Netzsch STA449C), and a confocal microprobe Raman system (LabRam-010, 632 nm as excitation source). They also were observed by FESEM (Hitachi, S-4800) and TEM (JEOL, JEM-2010).

Electrochemical measurements

The electrochemical experimental methods used in this work were similar to the ones in our previous study.[14] The electrochemical properties of the samples were tested using CR2016 coin cells. The active materials (nanocomposites or bare SnS) were mixed with carbon black and carboxylmethyl cellulose in a weight ratio of 8 : 1 : 1 with water as a dispersant. The mass of active material on each anode was *ca.* 0.8 mg. Lithium foils were used as counter electrodes. A Celgard 2400 microporous polypropylene membrane was used as a separator. The electrolyte consisted of a solution of 1 M $LiPF_6$ in ethylene carbonate–dimethyl carbonate–diethyl carbonate (1 : 1 : 1, in wt%). Coin-type cells were assembled in an argon-filled glove-box with water and oxygen contents of less than 1 ppm. The discharge and charge measurements were carried on an Arbin BT2000 system with the cut off potentials being 0.02 V for discharge and 2.5 V for charge. All of the specific capacities in this study were calculated based on the mass of active materials (SnS_x–G, or bare SnS).

3 Results and discussion

SnS_x–G nanocomposites were prepared by a hydrothermal method. In a comparison experiment, GO was not added, and the samples were collected and marked as SnS_x-1. The experimental details are shown in the ESI†. To verify whether Sn^{2+} could be oxidized by GO or not, SnS_x–G and SnS_x-1 were characterized by XRD, and the results are shown in Fig. 1a and b. As shown in Fig. 1a, the diffraction pattern and relative intensities of SnS_x-1 match well with those of SnS (JCPDS#39-354), demonstrating that SnS_x-1 is pure SnS. In comparison, most of the strong diffraction peaks in SnS_x–G could be indexed to the standard diffraction data of hexagonal SnS_2 (JCPDS#23-677) with the exception of a few weak peaks that are marked by stars. Those weak peaks could be attributed to SnS, arising from unoxidized stannous ions. Thus, the above results suggest that stannous ions are oxidized by GO to form SnS_2.

SnS_x–G nanocomposites were further characterized by FTIR and Raman spectroscopy, as displayed in Fig. 1c and d. The FTIR spectra verify the presence of some oxygen-containing groups in GO, such as C–OH (3390 cm^{-1}), C–O–C (1230 cm^{-1}), and C=O in carboxylic acid moieties (1730 cm^{-1}). The peak at 1620 cm^{-1} is assigned to the contributions from the skeletal vibrations of the graphitic domains.[20] All of the peaks in GO are similar to those in published papers.[19] As expected, there is no carboxylic acid vibration band (1730 cm^{-1}) in the FTIR spectrum of SnS_x–G. A small peak was found at about 1230 cm^{-1}, which was attributed to C–O–C. Only a weak signal for the C–OH stretching vibration at 3440 cm^{-1} could be found, which could be ascribed to the vibrations of the adsorbed water molecules. Therefore, GO was reduced while the stannous ions were oxidized. Digital photographs of the aqueous dispersion of GO and graphene sheets (GSs), which are prepared from SnS_x–G (as shown in ESI†), are shown in Fig. 1e. The color of the aqueous colloidal suspension changed from yellow-brown (GO) to homogeneous black (GSs), also demonstrating that GO was reduced by stannous ions.[21] In addition, XPS data in previous literature have demonstrated that either a hydrothermal process or stannous ions could be used to reduce graphene oxide to form graphene or its composites.[22,23]

Fig. 1d compares the Raman spectra of SnS_x–G and GO. The peak at about 1589 cm^{-1} (G band) is related to the vibration of the sp^2-bonded carbon atoms in a 2-dimensional hexagonal lattice, while the peak at about 1326 cm^{-1} (D band) is related to the defects and disorder in hexagonal graphitic layers.[24] The intensity ratio of the D to G band (I_D/I_G) is calculated as 1.10 for GO and 1.21 for SnS_x–G. It is generally accepted that the I_D/I_G

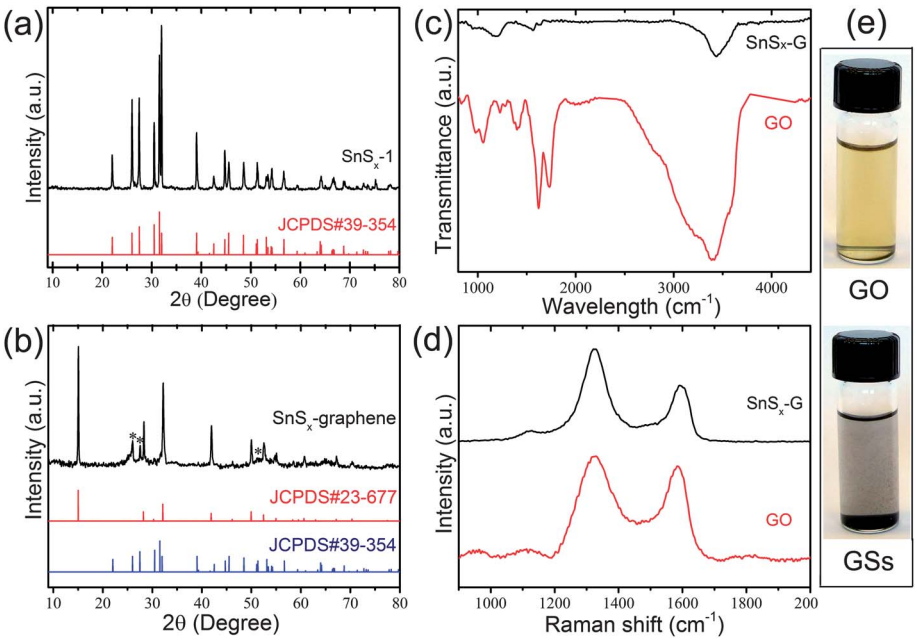

Fig. 1 (a) and (b) XRD patterns of SnS and SnS_x–G; (c) and (d) FTIR and Raman spectra of GO and SnS_x–G; (e) digital photographs of the aqueous dispersions of GO and GSs.

ratio reflects the graphitization degree of carbonaceous materials and also the defect density.[25] It is obvious that the I_D/I_G for SnS_x–G increases slightly compared with GO, and this value is much larger than that for graphene obtained *via* CVD.[26] The enhancement could be ascribed to the exfoliation of GO and the presence of SnS_x nanoparticles between GSs.

Although the successful synthesis of SnS_x–G nanocomposites is unambiguously confirmed experimentally, the exact chemical reactions for the oxidization of Sn^{2+} and the formation of SnS_x–G nanocomposites are less clear. The following are some possible proposed chemical reactions. Firstly, GO sheets were exfoliated by sonicating and some oxygen-containing groups (possibly hydroxyls, carboxyls or epoxys) interacted with water molecules, as shown in Fig. 2. Under the synthesis conditions employed in the present research, the GO surface was to be negatively charged, and Sn^{2+} cations were electrostatically attracted and captured by oxygen functional groups on the GO surface (eqn (1)).[27] Thirdly, thiourea was hydrolyzed at a high temperature, as described in eqn (2).[28,29] Subsequently, Sn^{2+} was oxidized to produce SnS_2 and GO was reduced to graphene simultaneously (eqn (3)), which has been demonstrated by XRD patterns and FTIR spectra of SnS_x–G, and the digital photograph of GSs.

$$Sn^{2+} + GO \rightarrow Sn^{2+}/GO \quad (1)$$

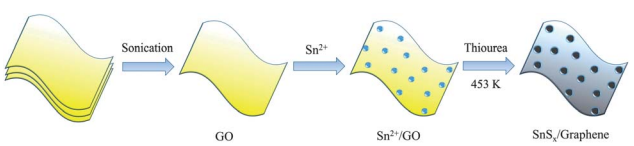

Fig. 2 Schematic illustration of the synthesis of SnS_x–G nanocomposites *via* oxidizing Sn^{2+} by GO and thiourea in aqueous solution under hydrothermal conditions.

$$CS(NH_2)_2 + 2H_2O \rightarrow H_2S + 2NH_3 + CO_3 \quad (2)$$

$$Sn^{2+}/GO + H_2S \rightarrow SnS_x\text{–graphene} + H_2O\ (1 < x < 2) \quad (3)$$

The morphology and microstructure of SnS_x–G were characterized using field emission scanning electron microscopy (FESEM) and transmission electron microscopy (TEM). As displayed in Fig. 3a, SnS_x–G nanocomposites are composed of GSs and nanoparticles, which look like stars dotting the sky. Fig. 3b shows a magnified image of SnS_x–G, showing that the diameters of those nanoparticles are about 5 nm. This value is less than that (about 10 nm) of SnS_2 in another report about SnS_2–graphene composites, which were synthesized by a similar hydrothermal method.[18] The difference between our method and the published one is that the concentration (15 mM) of tin ions in this study is much lower than that (80 mM) of previous research. It was demonstrated in a previous paper that with a lower concentration of tin ions in solution, smaller tin sulfide particles were formed when the ratio of tin to sulfur was constant.[30] Therefore, it is not difficult to understand that the size of the tin sulfide nanoparticles in this study is much smaller than in published results. In addition, the absence of charging during FESEM characterization implies the nanocomposites are of high conductivity, indicating the transformation of GO to graphene.

TEM images of the nanocomposites are shown in Fig. 3c and d. A sheet-like graphene is obvious in Fig. 3c. It looks like a crumpled piece of wrinkled thin paper with a lot of folds at the edge. Moreover, a variety of nanoparticles are loaded on GSs even after processing by sonication for TEM observation, indicating a firm connection between the nanoparticles and the GSs. A high resolution transmission electron microscopy image is shown in Fig. 3d. Three nanoparticles, which are marked by dotted cycles, could be seen in this image. Regular lattice fringes

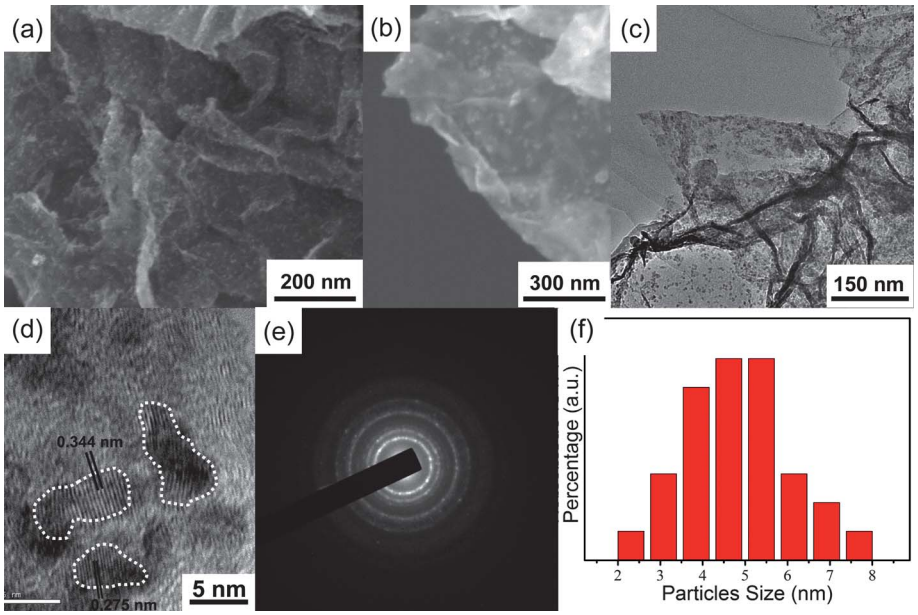

Fig. 3 (a) and (b) FESEM images of SnS_x–G at different magnification; (c) and (d) TEM images of SnS_x–G; (e) SAED of SnS_x–G; (f) the size distribution of SnS_x.

with spacings of 0.278 and 0.342 nm are highly consistent with the *d* value of the (101) plane of SnS_2 (JCPDS#23-677) and the (120) plane of SnS (JCPDS#39-354), respectively. Those results indicate that the nanocomposites consist of SnS and SnS_2 nanoparticles. Furthermore, the distinct ring pattern of the selected-area electron diffraction (SAED), as displayed in Fig. 3e, reveals the polycrystalline nature of the nanoparticles. Fig. 3f shows the size distribution of SnS_x nanoparticles according to TEM images. It clearly shows that the average particle size was about 5 nm, matching well with the results of FESEM characterization. Thermogravimetric analysis was employed to evaluate the mass ratio of SnS_x–G nanocomposites. Based on the results shown in Fig. S1 (ESI†), the mass ratio of SnS_x in the nanocomposites could be roughly calculated to be 80%.

To understand the electrochemical reaction mechanism of SnS_x–G as anodes for LIBs, the cyclic voltammogram (CV) profiles of coin cells were characterized, as displayed in Fig. 4a and b. During the first cycle, cathodic peaks of SnS appear at about 0.8 and 0.1 V, and anodic peaks appear at about 0.7 and 2.0 V (Fig. 4a). The cathodic peak at about 0.8 V can be assigned to two aspects: the decomposition of SnS_x (eqn (4)) and the formation of a solid electrolyte interface (SEI), which is responsible for the irreversible capacity in the first cycles.[31] Another cathodic peak at 0.1 V represents the reaction shown in eqn (5). During the anodic sweep, the delithiation peak of Sn–Li alloy is at about 0.7 V. It should be noted that there is another anodic peak at about 2.0 V, which may be assigned to the transformation of Li_2S to polysulfides.[32,33] Its peak current decreases gradually in following cycles. The cathodic peak at about 1.2 V also becomes weak, showing the partial reversibility of delithiating Li_2S. Similar results could be found in previous literature on SnS as an anode material for LIBs.[34] The CV curves of SnS_x–G are displayed in Fig. 4b, which are different from those of SnS. The cathodic peak at about 0 V could be attributed to the storage of lithium on graphene sheets. Additionally, there are two obvious anodic peaks. Three peak currents (including a cathodic peak and two anodic peaks) are unchanged from the second cycle, suggesting the good cycling stability of SnS_x–G. Previous reports have shown that both S and Li_2S were electrochemical activated materials for LIBs.[32,33] So, taking into account the small size of SnS_x in nanocomposites (about 5 nm, much smaller than the size of tin sulfide in other SnS_2–graphene),[18] the anodic peak at 1.35 V is believed to be the reversible delithiation of Li_2S,[35] which has a theoretical capacity of 1166 mA h g^{-1}.[36] Based on this new mechanism, the theoretical capacities of SnS and SnS_2 toward the storage of lithium ions are calculated to be 1138 and 1231 mA h g^{-1}, respectively. All of these values are higher than those of SnS and SnS_2 according to the traditional mechanism.

$$SnS_x + 2xLi \rightleftharpoons Sn + xLi_2S\ (1 < x < 2) \quad (4)$$

$$Sn + yLi \rightleftharpoons SnLi_y\ (1 \leq y \leq 2) \quad (5)$$

The electrochemical performances of SnS_x–G were further investigated. Fig. 4c shows the first discharge–charge curves of anodes based on SnS_x–G (A and B) and SnS (C and D). In the discharge process, the plateaus at about 1.0 V in both curves A and C show the decomposition of SnS_x, corresponding to the cathodic peaks in CV measurements. During the anodic sweep, two plateaus at about 0.5 and 1.9 V are found in curve D, resulting from the reaction in eqn (5) and the delithiation of Li_2S. However, the anodic plateaus of SnS_x–G are different from those of SnS, which are at about 0.5 and 1.2 V. The plateau of SnS_x–G corresponding to the delithiation of Li_2S is lower than that of SnS, indicating that Li_2S arising from SnS_x–G is easier to decompose. This may be attributed to the very small size of SnS_x in the nanocomposites and the good

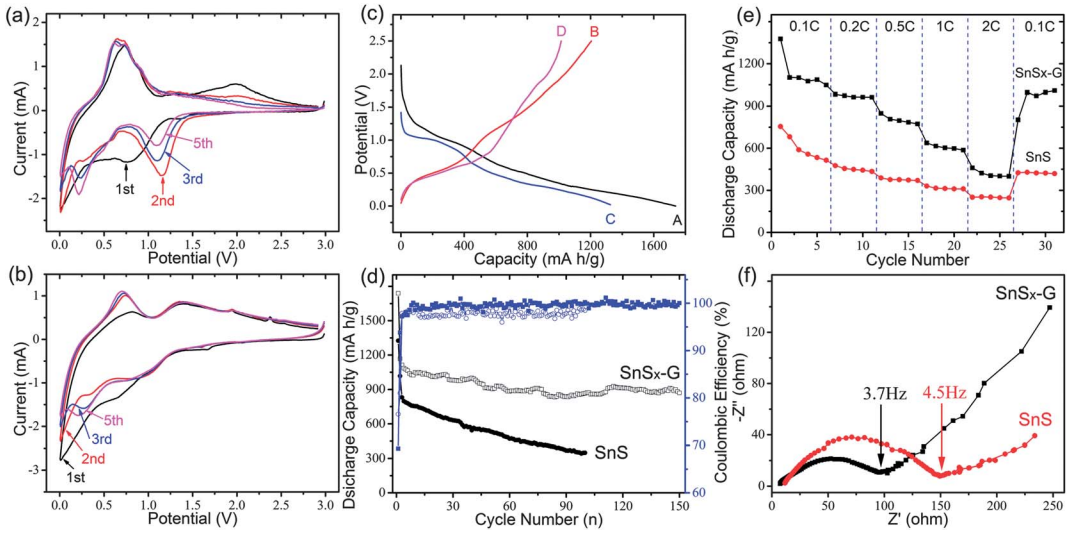

Fig. 4 (a) and (b) CV curves of SnS and SnS_x–G; (c) discharge–charge profiles of SnS_x–G (A, B) and SnS (C and D) in the first cycle; (d) cycling performance and coulombic efficiencies of SnS_x–G and SnS; (e) rate capacities of SnS and SnS_x–G; (f) AC impedance plots for SnS and SnS_x–G after tests of rate capacities.

conductance of the nanocomposites arising from GSs, which may dramatically improve the electrochemical kinetics of the sulfur (and Li_2S) in LIBs.[32] These results agree well with the results of the CVs, demonstrating the reversibility of decomposing Li_2S in SnS_x–G nanocomposites.

The cycling performances of SnS and SnS_x–G were evaluated over a potential range of 0.02–2.5 V (*vs.* Li^+/Li) at 0.2 C (discharge–charge of all active materials within 5 h), and the results are displayed in Fig. 4d. SnS_x–G exhibits larger discharge and charge capacities of about 1738 and 1205 mA h g^{-1} in the first cycle compared with SnS, corresponding to a coulombic efficiency of about 69%. During the following cycles, the coulombic efficiencies of SnS_x–G are a bit higher than those of SnS. Thus, it could be shown that SnS_x–G nanocomposites manifest excellent capacity retention of 865 mA h g^{-1} after 100 cycles and 860 mA h g^{-1} after 150 cycles. These values are higher than those of SnS with a discharge capacity of 350 mA h g^{-1} after 100 cycles. The results are also good in comparison with previous results for tin sulfide as an anode for LIBs,[15–17,28,30,31,34,37–51] (as shown in Table 1). In addition, those values also are higher than the theoretical capacity of SnS_2 and SnS based on an alloying mechanism. The improved cycling performance of SnS_x–G could be ascribed to a new mechanism of decomposing Li_2S at a relative low potential, as shown in Fig. 4b. Besides, GSs with good conductance and superior flexibility have a positive effect on the structural stability and electron transfer, resulting in a good cycling performance. Another reason for the superior performance of SnS_x–G could be attributed to GSs which could control the growth and suppress the aggregation of tin nanoparticles.[52]

To comprehensively investigate the electrochemical performance of SnS_x–G nanocomposites, their rate capacities were characterized and the results are shown in Fig. 4e. The rate capacities of SnS_x–G are higher than those of SnS at all testing rates. Even at a rate of 2 C, SnS_x–G could deliver a reversible capacity of 450 mA h g^{-1}. After the high rate measurement, SnS_x–G exhibited a capacity of 970 mA h g^{-1} at a rate of 0.1 C, which was almost 2.3 times that of SnS. These results show that SnS_x–G nanocomposites are superior materials for LIBs. To investigate the reason why SnS_x–G nanocomposites have superior rate capacities, Nyquist plots of the AC impedance were

Table 1 Specific capacities of tin sulfide based materials as anode materials for LIBs

	Reversible capacity at different cycle[c]			
Material	30^{th}	50^{th}	Other	Ref.
SnS_2	600 (25^{th})			31
SnS_2		400 (60^{th})		30
SnS		300		37
SnS_2		380		
SnS		400 (40^{th})		38
SnS		484 (40^{th})		39
SnS_2		500		35
SnS	200 (24^{th})			40
SnS_2	280 (14^{th})			
SnS/C		542 (40^{th})		34
SnS_2	580			41
SnS_2/C		668		42
SnS		780		43
SnS_2		700 (40^{th})		44
SnS_2		502		28
SnS_2		513		45
SnS	620 (15^{th})			46
SnS_2			570	47
SnS_2		390		50
SnS_2–G[a]	650			15
SnS_2–G		350		17
SnS_2–G		920		16
SnS_2–G	400 (25^{th})			18
SnS_2–G	1110			48
SnS_2–G			500 (200^{th})	49
SnS_2–G			405 (80^{th})	51
SnS_x–G[b]			860 (150^{th})	This work

[a] SnS_2–graphene. [b] SnS_x–graphene ($1 < x < 2$). [c] Unit: mA h g^{-1}.

measured after the tests of rate capacities. As shown in Fig. 4f, the impedance spectra show two partially overlapped semicircles at the high- and medium-frequency range, which describe the SEI layer resistance (R_{SEI}) and the charge transfer resistance (R_{ct}) for both electrodes.[53–55] An inclined line in the low frequency range is observed, which could be considered as Warburg impedance. It is clear that the sizes of semicircles for SnS_x–G are smaller than those for SnS, indicating lower R_{SEI} and R_{ct} of SnS_x–G. Therefore, the excellent electrochemical performance of SnS_x–G could be attributed to the interleaved electron transfer highways built up by GSs and lower R_{SEI} arising from GSs. The structure of SnS_x nanoparticles with small sizes dotted on GSs resulted in wonderful electron delivery between SnS_x nanoparticles and GSs. This may be another reason for the excellent performance of SnS_x–G nanocomposites.

4 Conclusions

In conclusion, for the first time, SnS_x–G nanocomposites with excellent Li^+ storage properties were synthesized *via in situ* oxidization of stannous ions by GO acting as both the oxidizer and the precursor of graphene. The size of SnS_x in SnS_x–G composites was tailored to as small as 5 nm on average. With this unique microstructure, SnS_x–G may host Li^+ by a new mechanism that Li_2S arising from SnS_x could be reversibly delithiated at a relatively low potential to storage lithium. Based on this novel mechanism, SnS_x–G exhibited a discharge capacity of 860 mA h g^{-1} after 150 cycles at a rate of 0.2 C and higher rate capacities than those of bare SnS nanoparticles and theoretical capacities of tin sulfide based on the traditional mechanism. In addition, GSs with superior conductivity, good flexibility and extraordinary stability may be another reason why SnS_x–G showed excellent electrochemical performance towards the storage of Li^+. It is believed that the strategy of synthesizing SnS_x–G by employing GO as oxidizer and a probably novel mechanism of Li^+ storage in SnS_x may open a new way for the synthesis of sulfide–graphene with significantly enhanced properties for the storage of Li^+.

Acknowledgements

This work was partly supported by the '973' National Key Basic Research Program of China (2007CB310500), the National Natural Science Foundation of China (21003041, 21103046), the Hunan Provincial Natural Science Foundation of China (10JJ1011and 11JJ7004) and the China Scholarship Council. This research has been also financially supported in part by the National Science Foundation (CMMI-1030048).

References

1 P. A. Denis, *J. Phys. Chem. C*, 2009, **113**, 5612.
2 S. Evers and L. F. Nazar, *Chem. Commun.*, 2012, **48**, 1233.
3 D. H. Wang, D. Choi, J. Li, Z. Yang, Z. Nie, R. Kou, D. Hu, C. Wang, L. V. Saraf, J. Zhang, I. A. Aksay and J. Liu, *ACS Nano*, 2009, **3**, 907.
4 S. Stankovich, D. A. Dikin, G. H. B. Dommett, K. M. Kohlhaas, E. J. Zimney, E. A. Stach, R. D. Piner, S. T. Nguyen and R. S. Ruoff, *Nature*, 2006, **442**, 282.
5 J. S. Chen, Z. Wang, X. C. Dong, P. Chen and X. W. Lou, *Nanoscale*, 2011, **3**, 2158.
6 S. Ding, D. Luan, F. Y. C. Boey, J. S. Chen and X. W. Lou, *Chem. Commun.*, 2011, **47**, 7155.
7 Z. Lin, Y. Liu, Y. Yao, O. J. Hildreth, Z. Li, K. Moon and C. P. Wong, *J. Phys. Chem. C*, 2011, **115**, 7120.
8 A. Kaniyoor and S. Ramaprabhu, *J. Mater. Chem.*, 2012, **22**, 8377.
9 B. Y. Xia, B. Wang, H. B. Wu, Z. Liu, X. Wang and X. W. Lou, *J. Mater. Chem.*, 2012, **22**, 16499.
10 J. Liang, Y. Huang, J. Oh, M. Kozlov, D. Shi, S. Fang, R. H. Baughman, Y. Ma and Y. S. Chen, *Adv. Funct. Mater.*, 2011, **21**, 3778.
11 L. Ji, Z. Tan, T. Kuykendall, E. J. An, Y. Fu, V. Battaglia and Y. Zhang, *Energy Environ. Sci.*, 2011, **4**, 3611.
12 X. Huang, K. Qian, J. Yang, J. Zhang, L. Li, C. Yu and D. Zhao, *Adv. Mater.*, 2012, **24**, 4419.
13 M. Zhang, D. Lei, X. Yin, L. Chen, Q. Li, Y. Wang and T. Wang, *J. Mater. Chem.*, 2010, **20**, 5538.
14 M. Zhang, B. Qu, D. Lei, Y. Chen, X. Yu, L. Chen, Q. Li, Y. Wang and T. Wang, *J. Mater. Chem.*, 2012, **22**, 3868.
15 B. Luo, Y. Fang, B. Wang, J. Zhou, H. Song and L. J. Zhi, *Energy Environ. Sci.*, 2012, **5**, 5226.
16 K. Chang, Z. Wang, G. Huang, H. Li, W. X. Chen and J. Y. Lee, *J. Power Sources*, 2012, **201**, 259.
17 C. Shen, L. Ma, M. B. Zheng, B. Zhao, D. Qiu, L. Pan, J. Cao and Y. Shi, *J. Solid State Electrochem.*, 2012, **16**, 1999.
18 M. Sathish, S. Mitani, T. Tomai, A. Unemoto and I. Honma, *J. Solid State Electrochem.*, 2012, **16**, 1767.
19 M. Zhang, S. Liu, X. Yin, Z. Du, Q. Hao, D. Lei, Q. Li and T. Wang, *Chem.–Asian J.*, 2011, **6**, 1151.
20 Y. Liang, D. Wu, X. L. Feng and K. Mullen, *Adv. Mater.*, 2009, **21**, 1679.
21 J. Gao, F. Liu, Y. Liu, N. Ma, Z. Wang and X. Zhang, *Chem. Mater.*, 2010, **22**, 2213.
22 Y. Zhou, Q. Bao, L. A. L. Tang, Y. Zhong and K. P. Loh, *Chem. Mater.*, 2009, **21**, 2950.
23 Y. Li, X. Lv, J. Lu and J. Li, *J. Phys. Chem. C*, 2010, **114**, 21770.
24 A. C. Ferrari, J. C. Meyer, V. Scardaci, C. Casiraghi, M. Lazzeri, F. Mauri, S. Piscanec, D. Jiang, K. S. Novoselov, S. Roth and A. K. Geim, *Phys. Rev. Lett.*, 2006, **97**, 187401.
25 W. Lin, K. S. Moon, S. Zhang, Y. Ding, J. Shang, M. Chen and C. P. Wong, *ACS Nano*, 2010, **4**, 1716.
26 A. Reina, X. Jia, J. Ho, D. Nezich, H. Son, V. Bulovic, M. S. Dresselhaus and J. Kong, *Nano Lett.*, 2009, **9**, 30.
27 M. Zhang, D. Lei, Z. Du, X. Yin, L. Chen, Q. Li, Y. Wang and T. Wang, *J. Mater. Chem.*, 2011, **21**, 1673.
28 S. Liu, X. Yin, L. Chen, Q. Li and T. Wang, *Solid State Sci.*, 2010, **12**, 712.
29 J. Bu, C. Nie, J. Liang, L. Sun, Z. Xie, Q. Wu and C. Lin, *Nanotechnology*, 2011, **22**, 125602.
30 H. Mukaibo, A. Yoshizawa, T. Momma and T. Osaka, *J. Power Sources*, 2003, **119**, 60.
31 T. Momma, N. Shiraishi, A. Yoshizawa, T. Osaka, A. Gedanken, J. Zhu and L. Sominshi, *J. Power Sources*, 2001, **87**, 198.
32 J. L. Wang, J. Yang, C. Wan, K. Du, J. Xie and N. Xu, *Adv. Funct. Mater.*, 2003, **13**, 487.
33 L. Ji, M. Rao, H. Zheng, L. Zhang, Y. Li, W. Duan, J. Guo, E. J. Cairns and Y. G. Zhang, *J. Am. Chem. Soc.*, 2011, **133**, 18522.
34 Y. Li, J. P. Tu, X. H. Huang, H. M. Wu and Y. F. Yuan, *Electrochem. Commun.*, 2007, **9**, 49.
35 T. J. Kim, C. Kim, D. Son, M. Choi and B. Park, *J. Power Sources*, 2007, **167**, 529.
36 Y. Yang, M. T. McDowell, A. Jackson, J. J. Cha, S. S. Hong and Y. Cui, *Nano Lett.*, 2010, **10**, 1486.
37 X. L. Gou, J. Chen and P. W. Shen, *Mater. Chem. Phys.*, 2005, **93**, 557.
38 Y. Li, J. P. Tu, H. M. Wu, Y. F. Yuan and D. Q. Shi, *Mater. Sci. Eng., B*, 2006, **128**, 75.
39 Y. Li, J. P. Tu, X. H. Huang, H. M. Wu and Y. F. Yuan, *Electrochim. Acta*, 2006, **52**, 1383.
40 C. R. Patra, A. Odani, V. G. Pol, D. Aurbach and A. Gedanken, *J. Solid State Electrochem.*, 2007, **11**, 186.
41 J. W. Seo, J. T. Jang, S. W. Park, C. Kim, B. Park and J. Cheon, *Adv. Mater.*, 2008, **20**, 4269.
42 H. S. Kim, Y. H. Chung, S. H. Kang and Y. E. Sung, *Electrochim. Acta*, 2009, **54**, 3606.

43 J. G. Kang, J. G. Park and D. W. Kim, *Electrochem. Commun.*, 2010, **12**, 307.
44 S. Liu, X. Yin, Q. Hao, M. Zhang, L. Li, L. Chen, Q. Li, Y. Wang and T. Wang, *Mater. Lett.*, 2010, **64**, 2350.
45 C. Zhai, N. Du, H. Zhang and D. Yang, *Chem. Commun.*, 2011, **47**, 1270.
46 K. Aso, A. Hayashi and M. Tatsumisago, *Cryst. Growth Des.*, 2011, **11**, 3900.
47 J. Zai, K. Wang, Y. Su, X. F. Qian and J. Chen, *J. Power Sources*, 2011, **196**, 3650.
48 L. Zhuo, Y. Wu, L. Wang, Y. Yu, X. Zhang and F. Zhao, *RSC Adv.*, 2012, **2**, 5084.
49 Z. Jiang, C. Wang, G. Du, Y. J. Zhong and J. Z. Jiang, *J. Mater. Chem.*, 2012, **22**, 9494.
50 J. Ma, D. Lei, X. Duan, Q. Li, T. Wang, A. Cao, Y. Mao and W. Zheng, *RSC Adv.*, 2012, **2**, 3615.
51 L. Ji, H. L. Xin, T. R. Kuykendall, S. L. Wu, H. Zheng, M. Rao, E. J. Cairns, V. Battaglia and Y. Zhang, *Phys. Chem. Chem. Phys.*, 2012, **14**, 6981.
52 H. Wang, H. S. Casalongue, Y. Liang and H. Dai, *J. Am. Chem. Soc.*, 2010, **132**, 7472.
53 J. Wang, J. Chen, K. Konstantinov, L. Zhao, S. H. Ng, G. X. Wang, Z. P. Guo and H. K. Liu, *Electrochim. Acta*, 2006, **51**, 4634.
54 D. Liu, Y. Liu, B. B. Garcia, Q. F. Zhang, A. Pan, Y. H. Jeong and G. Z. Cao, *J. Mater. Chem.*, 2009, **19**, 8789.
55 M. Umeda, K. Dokko, Y. Fujita, M. Mohamedi, I. Uchida and J. R. Selman, *Electrochim. Acta*, 2001, **47**, 885.